nature nanotechnology

ARTICLES

PUBLISHED ONLINE: 3 AUGUST 2014 | DOI: 10.1038/NNANO.2014.154

A carbon nanotube–polymer composite for T-cell therapy

Tarek R. Fadel[1], Fiona A. Sharp[2], Nalini Vudattu[3†], Ragy Ragheb[2], Justin Garyu[3†], Dongin Kim[2], Enping Hong[2], Nan Li[1], Gary L. Haller[1], Lisa D. Pfefferle[1], Sune Justesen[4], Kevin C. Harold[3] and Tarek M. Fahmy[1,2,3]*

Clinical translation of cell therapies requires strategies that can manufacture cells efficiently and economically. One promising way to reproducibly expand T cells for cancer therapy is by attaching the stimuli for T cells onto artificial substrates with high surface area. Here, we show that a carbon nanotube–polymer composite can act as an artificial antigen-presenting cell to efficiently expand the number of T cells isolated from mice. We attach antigens onto bundled carbon nanotubes and combined this complex with polymer nanoparticles containing magnetite and the T-cell growth factor interleukin-2 (IL-2). The number of T cells obtained was comparable to clinical standards using a thousand-fold less soluble IL-2. T cells obtained from this expansion were able to delay tumour growth in a murine model for melanoma. Our results show that this composite is a useful platform for generating large numbers of cytotoxic T cells for cancer immunotherapy.

A goal of successful cancer immunotherapy is the stimulation of T cells against tumour targets[1]. A promising method for this purpose is adoptive cell-transfer therapy[2]. This technique relies on the *ex vivo* expansion and infusion of tumour-specific T cells from patients' blood. A lack of efficient procedures for expansion of the cells currently limits the application of this therapy, but this may be overcome by the engineering of a new generation of devices for T-cell expansion and enrichment[3]. One example is the recent use of synthetic biology to engineer antibody fragments in T cells[4,5]. These T cells have been shown to provide long-lasting therapeutic effects for relapsed or refractory B-cell acute lymphoblastic leukaemia[6].

Effective immunity requires that antigen-specific lymphocytes undergo activation, expansion and differentiation through interaction with antigen-presenting cells (APCs) such as dendritic cells (DCs)[7]. These DCs can be used to initiate potent immune responses, but cost and time-dependent factors related to their procurement and production have limited their widespread use[8,9]. It is known that natural antigen presentation involves avid interactions with T cells[10,11], leading to efficient stimulation[12,13]. Regions with a high density of T-cell antigen receptors have been termed immunological synapses[14,15] because they are critical for lymphocyte stimulation[16,17]. Antigen density is also important on the organ scale. In the lymph node, the primary site for T-cell stimulation, APCs concentrate antigen in dense regions in close proximity to T cells. For this reason, high-antigen-density platforms such as magnetic beads[18], liposomes[19], exosomes[20], biodegradable polymer particles[21] and latex beads[22] have been proposed as artificial APCs (aAPCs)[8]. Finally, cytokines—the largest class of immunoregulatory molecules—play a critical role in long-term T-cell expansion[7]. For example, IL-2 is a key signal for T-cell cluster initiation and persistence after antigen priming[23]. It is secreted in paracrine fashion at the interface between a T cell and an APC upon contact[24], and has been used as a component of cell-based immunotherapies[25,26].

Here, we report a carbon nanotube–polymer composite (CNP) that can function as an efficient aAPC for expanding T cells for cancer immunotherapy. Carbon nanotubes (CNTs) were selected as the base nanomaterial because of their pronounced aspect ratio, which provides a unique nanometre-scale topography, a feature previously shown to enhance cell–cell interactions and long-term cultures[27–29]. The topography of CNTs facilitates a clustered presentation of T-cell stimuli, peptide-loaded major histocompatibility complex class-I (MHC-I), and the co-stimulatory ligand anti-CD28 (αCD28). Furthermore, the polymer component of the composite allows for paracrine delivery of IL-2[30], which is encapsulated in biotinylated poly(lactide-co-glycolide) (PLGA) nanoparticles together with magnetite. Magnetite is used here for enrichment of the CNP-expanded T cells by magnetic separation. Our results indicate that the carbon nanotube–polymer composite expands cytotoxic T cells *in vitro* to a level comparable to clinical standards using 1,000-fold less soluble IL-2. Furthermore, expanded lymphocytes are shown to significantly delay tumour growth in a murine melanoma model two weeks after tumour inoculation. We further demonstrate the application of the CNP with human cells. Compared to human DCs, CNPs show greater expansion of human Epstein–Barr Virus (EBV)-specific $CD8^+$ T cells. These results demonstrate the promise of this composite platform for T-cell cancer immunotherapy.

Synthesis and characterization of CNPs

The synthesis and functionalization of CNTs have previously been shown to yield ultrapure, hydroxyl-modified bundled nanotubes that are rich in surface defects and present a high surface area[31,32]. In the scheme shown in Fig. 1a, the protein linker neutravidin was adsorbed onto CNTs to yield neutravidin-bound CNTs (^{N}CNTs). Stoichiometric amounts of biotinylated T-cell stimulatory signals were then bound to the surface. This simple method enables stable presentation of different T-cell antigens[33]. A third crucial

[1]Department of Chemical Engineering, Yale University, PO Box 208284, New Haven, Connecticut 06511, USA, [2]Department of Biomedical Engineering, Yale University, PO Box 208284, New Haven, Connecticut 06511, USA, [3]Department of Immunobiology and Internal Medicine, Yale University, PO Box 208284, New Haven, Connecticut 06520, USA, [4]Department of Immunobiology and Microbiology, Blegdamsvej 3b DK2200, Copenhagen N Denmark, †These authors contributed equally to this work. *e-mail: tarek.fahmy@yale.edu

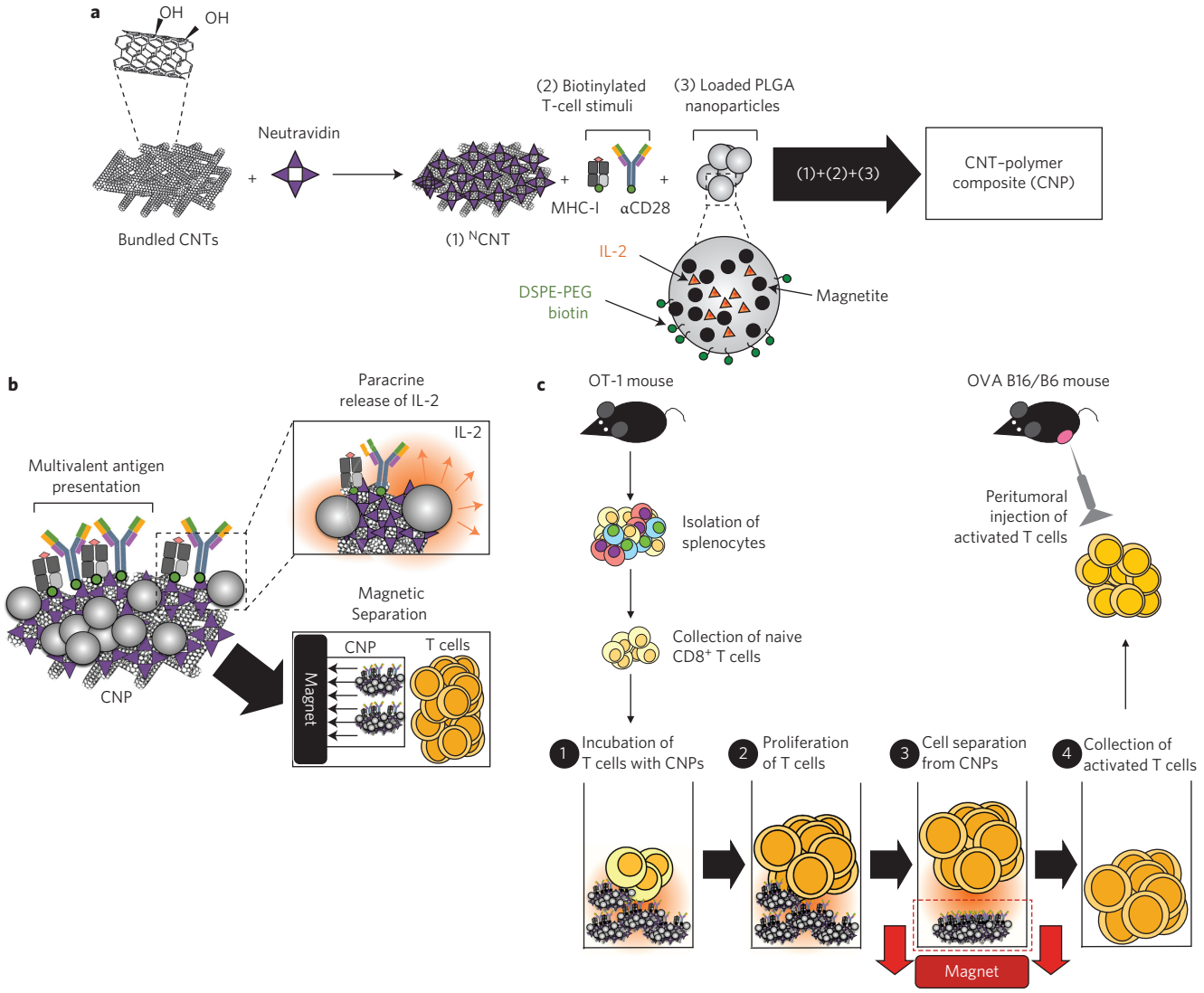

Figure 1 | Design of CNPs. Schematics describing the combination of multivalent antigen presentation, paracrine delivery of cytokine, and T-cell enrichment capabilities into CNPs. **a**, Schematic showing bundled CNTs binding neutravidin to present biotinylated T-cell stimuli and PLGA nanoparticles encapsulating magnetite and IL-2. **b**, Schematic highlighting three properties of the engineered CNP platform: multivalent antigen presentation, paracrine release of IL-2 and magnetic separation of CNPs from T cells. **c**, Work flow diagram depicting the T-cell stimulation process and cell separation using CNPs. OT-1 $CD8^+$ T cells were purified from splenocytes, and incubated with CNPs for three days. Activated T cells were then separated from CNPs and injected peritumorally into B6 mice, which had previously been inoculated with the B16 tumour for ten days.

signal involves paracrine delivery of cytokines to T cells. By binding PLGA nanoparticles co-encapsulating IL-2 and magnetite to ^{N}CNTs, we integrated the multivalent presentation of physiological T-cell stimuli with paracrine delivery of IL-2, while enabling the magnetic separation of CNPs from T cells (Fig. 1b). These features were tested by first stimulating ovalbumin-specific $CD8^+$ T cells directly isolated from transgenic mice (OT-1)[34]. Next, after magnetic separation from CNPs (Fig. 1c) we measured the therapeutic efficacy of those activated T cells in mice inoculated with melanoma cells expressing the ovalbumin antigen (B16-OVA).

The evolution of the platform from bundled CNTs to CNPs is shown in Fig. 2a,b. Structural gaps in the CNTs facilitate the adsorption of proteins (Fig. 2a) and nanoparticles (Fig. 2b, left panels). We first confirmed the encapsulation of magnetite in the PLGA nanoparticles and the qualitative binding of neutravidin-gold to bundled CNTs by transmission electron microscopy (TEM; Fig. 2b, right panels). The CNTs bundled into particles with a diameter of ~13 μm (Fig. 2c and Supplementary Fig. 1a) and were functionalized to introduce surface defects, resulting in a higher surface area (Table 1 and Supplementary Fig. 1b,c). The diameter of the PLGA nanoparticles was estimated to be ~264 nm (Fig. 2c). Biotin-PEG functionality on the nanoparticle surface was confirmed by ^{1}H NMR spectroscopy, with the presence of methylene protons from the PEG segment appearing at ~3.5 ppm (Supplementary Fig. 1d). As expected, the nanoparticles exhibited superparamagnetic properties at room temperature (Supplementary Fig. 1e). The adsorption isotherm of neutravidin on CNTs also demonstrated saturation at 8 nmol of protein/mg CNT (Supplementary Fig. 1f). Additional studies determined that optimal T-cell stimulation was achieved using 5 μg/ml ^{N}CNT, 125 μg/ml PLGA nanoparticles and a 2.1 nM concentration of biotinylated MHC-I and αCD28 (Supplementary Fig. 2). Comparing the $CD8^+$ T-cell response using avidin- or streptavidin-bound CNTs to ^{N}CNTs under similar experimental conditions indicated that, although the amount and distribution of protein is the same with all three platforms (Supplementary Fig. 3), the charge microenvironment provided by ^{N}CNTs was more optimal for the stimulation of T cells (Supplementary Fig. 4).

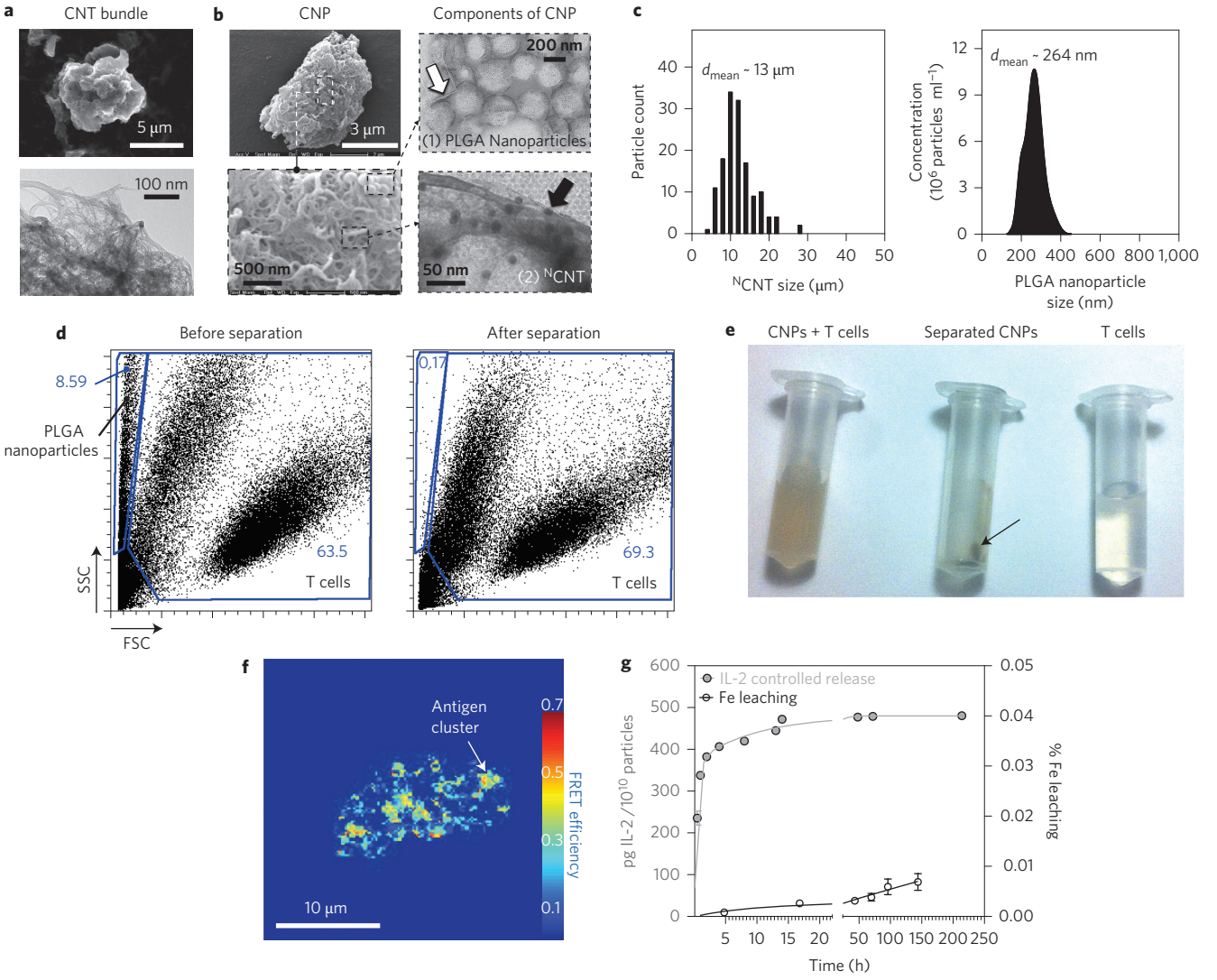

Figure 2 | Characterization of CNPs. CNP structure was characterized for size, magnetic separation, multivalent antigen presentation and release of cytokine. **a**, Scanning electron microscopy (SEM, top) and TEM (bottom) images of a CNT bundle. **b**, Left: SEM images of a CNP at low (top) and high (bottom) magnifications. Right: TEM images of PLGA nanoparticles (top) and ^{N}CNT (bottom). The white arrow points to magnetite nanoparticles encapsulated within the PLGA nanoparticles. The black arrow in the bottom image points to a gold neutravidin particle on ^{N}CNT. **c**, Size distribution of bundled CNT microparticles and PLGA nanoparticles measured from SEM images and using nanoparticle tracking analysis, respectively. Mean diameters are shown at the top of each plot. **d**, Scatter profiles for activated CD8^{+} T cells with CNPs before and after magnetic separation. The top left gate on each graph is drawn around the PLGA nanoparticles; the larger gate is drawn around CD8^{+} T cells. SSC, side scatter; FSC, forward scatter. **e**, Images of culture samples during the process of cell isolation. The black arrow points to the localization of CNPs where a magnetic field was applied. **f**, Representative FRET efficiency image for a ^{N}CNT substrate. The colour scale represents the degree of FRET efficiency from no clustering (0 value) to the highest measured FRET efficiency (0.7). Ten independent samples were measured per group. **g**, Measurement of encapsulated IL-2 (grey circles, left axis) and iron (empty circles, right axis) release from PLGA nanoparticles over a one-week period. The results are mean values from three independent experiments. Error bars represent ±s.e.m.

To investigate the impact of magnetite loading on IL-2 release from PLGA nanoparticles and subsequent T-cell stimulation, loading of magnetite was varied by wt% (6, 12 and 30 wt%; Table 2). We first observed a strong correlation between the wt% of magnetite (Supplementary Fig. 5a) and the number of PLGA nanoparticles encapsulating the magnetite (Supplementary Fig. 5b). For example, doubling the magnetite loading from 6 wt% to 12 wt% results in half as many particles, close to 8×10^{9} particles. Second, varying the wt% of magnetite co-encapsulated with the same amount of IL-2 in nanoparticles significantly affected the seven-day cumulative release of cytokine on a per-particle basis (Supplementary Fig. 5c). Third, CD8^{+} T cells incubated with CNPs at various wt% loadings of magnetite showed an optimal IFN-γ response at day 3 for particles loaded at 12 wt% when compared to other loadings at equal particle concentration (Supplementary Fig. 5d). Finally, the cell separation efficiency with the 12 wt% magnetite group was measured to be ~98% using flow cytometry and nanoparticle tracking analysis (Fig. 2d and Supplementary Fig. 5e,f). Images of samples before and after separation show successful separation of the CNPs from cells (Fig. 2e). To visualize and validate protein cluster formation on the surface of the CNT bundles, fluorescence resonance energy transfer (FRET) analysis was performed on the antigen-bound ^{N}CNT platform using acceptor photobleaching (Supplementary Fig. 6)[35]. The representative FRET efficiency map derived from the change in donor emission suggests the presence of several micrometre-scale antigen clusters with 60–70% FRET efficiencies (Fig. 2f). Finally, the presentation of biotin on PLGA nanoparticles was achieved using fatty acids and lipids as hydrophobic anchors to enable a high-density and long-lasting association with the PLGA matrix[36,37]. This

Table 1 | Physiochemical properties of two main components of CNP.

Property	Functionalized CNT	PLGA nanoparticles
Diameter	~0.8 nm/nanotube	~150–200 nm/particle
Length	~0.5–5 μm/tube ~20–40 μm/assembly	NA
Zeta potential (in H_2O)	-2.6 mV	-2.2 mV
Zeta potential (in buffer)	-26.4 mV	-5.0 mV
Surface group	1,610 m^2 g^{-1}	5×10^{-13} m^2/particle
Functional group	Hydroxyl	PEG-biotin
Magnetite loading	NA	12% by weight of PLGA
Protein loading	~8 nmol neutravidin/ 0.005 mg ml^{-1} CNT	~50 μg IL-2/100 mg PLGA
Concentration used in culture	5 μg ml^{-1}	125 μg ml^{-1}
Amount of antigen presented	2.1 nM	NA

NA, not applicable.

Table 2 | Effect of magnetite loading on magnetic separation, IL-2 release and T-cell stimulation.

	Per cent loading of magnetite in PLGA nanoparticles		
	6 wt%	12 wt%*	30 wt%
Per cent separation efficiency	72.5 ± 4.9	97.7 ± 1.0	95.8 ± 1.2
Il-2 released (pg/10^{10} particles)	773.5 ± 47.4	480.5 ± 9.2	293.9 ± 1.6
T-cell response (pg IFN-γ/ml)	1,622.5 ± 834.4	5,056.3 ± 595.7	3,122.5 ± 413.7

*These values highlight the results for the group selected in the paper (12 wt%).

biotinylation step further affords the attachment to ^{N}CNTs and allows co-encapsulation and prolonged retention of fatty acid-modified magnetite[38]. We measured the cumulative release of IL-2 and iron from PLGA nanoparticles loaded with 12 wt% magnetite (Fig. 2g). The controlled release profile of IL-2, measured over a period of more than a week, is typical of protein release during PLGA degradation[21]. It is characterized by an initial burst release followed by a continual release of protein over time. Leaching of iron from the particles was negligible over 150 h, and was measured to be below 0.01% of loaded iron.

In vitro stimulation of CD8$^+$ T-cell effectors by CNPs

We first examined the efficacy of CNPs as an aAPC by incubation with CD8$^+$ T cells isolated from an OT-1 mouse. Figure 3a compares expansion as a function of time for T cells interacting with CNPs; ^{N}CNTs, Dynabeads (commercially available magnetic beads) or soluble tetramers presenting antigens with exogenous IL-2 (^{N}CNT-EXO, DYNA-EXO and TET-EXO, respectively); and ^{N}CNTs, Dynabeads or soluble tetramers presenting antigens without the addition of IL-2 (^{N}CNT, DYNA and TET, respectively). After two weeks, CD8$^+$ T cells expanded ~200-fold, more than twice the cumulative expansion of cells interacting with DYNA-EXO, and more than four times that for TET-EXO. The sizing of cells interacting with these same platforms indicates that effects on expansion potentially extend to cell phenotype (Table 3). Finally, the measurement of IFN-γ released from these CD8$^+$ T cells parallels previous results on cell proliferation and size (Fig. 3b).

The early interaction of CD8$^+$ T cells with CNPs (Fig. 3c) is characterized by the formation of non-specific cell clusters around particles displaying MHC-I loaded with the null agonist peptide (SIYRYYGL) that does not trigger the OT-1 T-cell receptor (CNP/Null Agonist). Upregulation of effector markers was, however, observed in T cells interacting with CNPs presenting OT-1-specific antigens (MHC-I loaded with the peptide SIINFEKL). This was characterized by the presence of cytotoxic granules and the secretion of granzyme-B (Fig. 3c, top row, white arrow). Expression of CD25, the α-chain of the IL-2 receptor, was also observed at the T cell–CNP interphase. As expected, T cells cultured in the presence of CNP/Null Agonist did not express CD25 or granzyme-B. T cells incubated with soluble tetramers or Dynabeads expressed these effector markers (Fig. 3c, bottom two rows), although not to the same level of fluorescence intensity as observed with CNPs. T-cell cultures with CNPs displaying agonist peptide showed the formation of large cellular aggregates around the particle at 24 h, increasing in size through 48 and 72 h, as is characteristic of vigorous T-cell proliferation (Fig. 3d).

Flow cytometry analysis of activated cell phenotype indicated that a higher percentage of CD8$^+$ T cells expanded using CNPs retained expression of CD27 (a marker of T-cell expansion), CD69 (an early activation marker), CD25 (the IL-2 receptor) and CD62L (an L-selectin adhesion receptor on naive and central memory T cells). The percentage of CD8$^+$/CD27$^+$ T cells activated by CNPs was consistently above 90% during the first week of culture, and was significantly higher than the percentage of CD8$^+$/CD27$^+$ T cells generated by DYNA-EXO and TET-EXO at days 5, 7 and 14 (Fig. 4a and Supplementary Fig. 7b). Under the present culture conditions, at least 90% of CD8$^+$ T cells activated by CNPs were CD69$^+$/CD25$^+$ (Fig. 4b and Supplementary Fig. 7c), and a higher percentage of CD8$^+$ T cells expressing a CD44$^+$/CD62L$^+$ phenotype was sustained in the CNP group at days 7 and 14 (Fig. 4c and Supplementary Fig. 7d). Overall, T cells stimulated by CNPs were able to retain a stronger activated cell phenotype than controls (Supplementary Fig. 8). Expression of granzyme-B in T cells activated by CNPs was significantly higher than lymphocytes cultured with DYNA-EXO and TET-EXO (Fig. 4d and Supplementary Fig. 9). This is consistent with measurements of cell-specific cytolytic activity in lymphocytes previously expanded with CNPs and cultured with a melanoma tumour cell line (B16-OVA) (Fig. 4e). At an effector-to-target (E:T) ratio of 20:1, tumour cell lysis by T cells expanded with CNPs was as much as three times the cytolytic activity observed in cells expanded using commercially available magnetic beads supplemented with IL-2 in culture (DYNA-EXO).

Previous work has established the importance of IL-2 in increasing the proliferative capacity of T cells[39]. A recent study has demonstrated that at least 1,000-fold higher exogenous IL-2 concentration is required to match the effects of sustained paracrine delivery[30,40]. For this reason, we chose to approximate the observed effects of CNPs on CD8$^+$ T cells by adding 1,000-fold more exogenous IL-2 (62.5 ng ml^{-1}) in control groups, and to test the therapeutic efficacy of activated T cells in the context of a murine B16 melanoma model. Flow cytometry analysis of the expression of CD69 and CD25 from CD8$^+$ T cells cultured for three days with either CNPs and Dynabeads or soluble tetramers with 1,000-fold more IL-2 (DYNA-EXO$^+$ and TET-EXO$^+$, respectively)

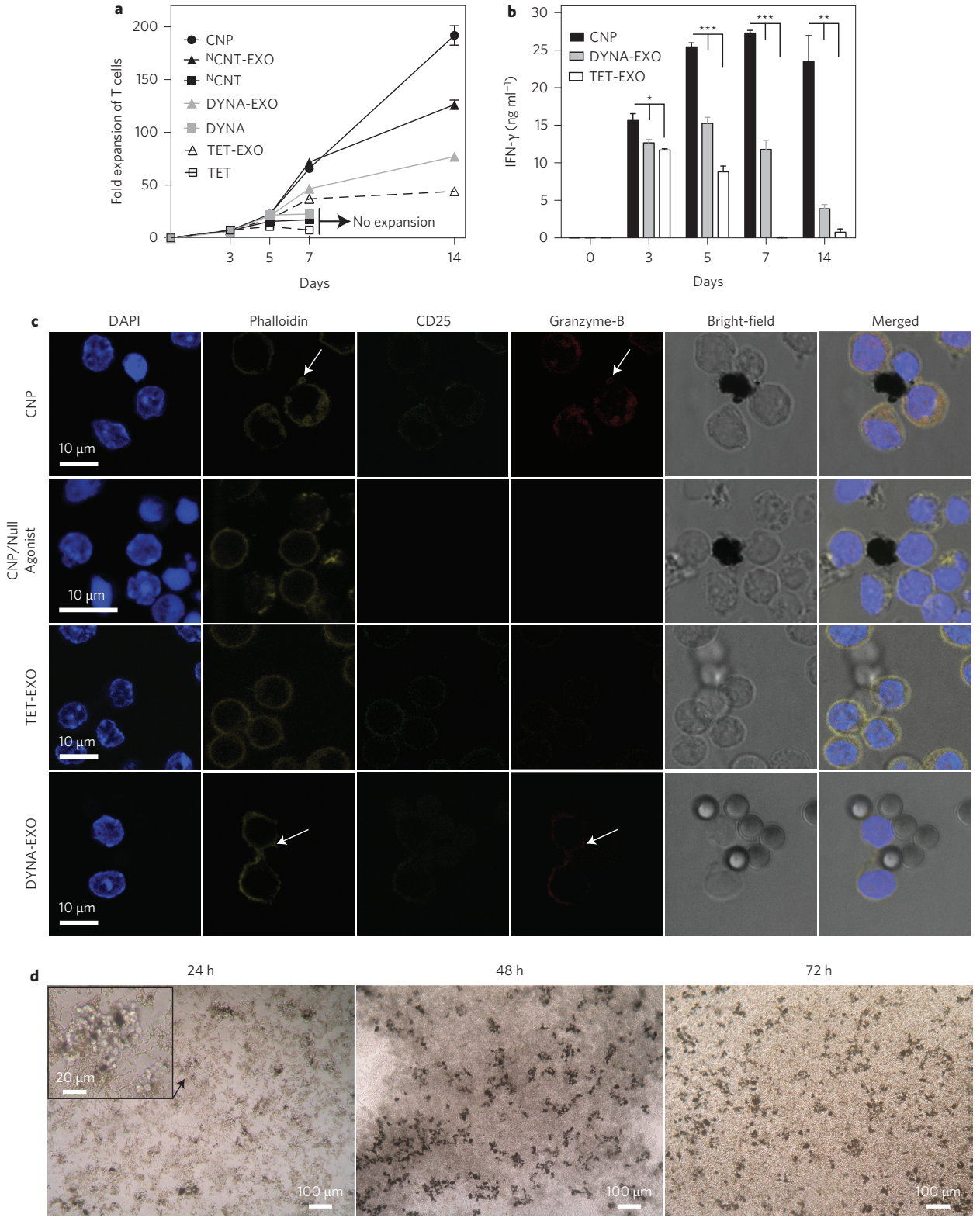

Figure 3 | CNPs enhance the long-term expansion of CD8$^+$ T cells. Measurement and visualization of T cells incubated with CNPs. **a**, Expansion of OT-1 CD8$^+$ T cells measured using a Coulter counter during a two-week period. The results are mean values from three independent experiments. Error bars represent ±s.d. **b**, IFN-γ release from OT-1 CD8$^+$ T cells measured at each time point during the two-week period. The results are mean values from three independent experiments. Error bars represent ±s.e.m. *$P < 0.05$, **$P < 0.01$, ***$P < 0.0001$. **c**, Confocal images of OT-1 CD8$^+$ T cells at 24 h interacting with, from top to bottom, CNP, CNP presenting a non-agonist antigen (labelled CNP/Null Agonist), TET-EXO and DYNA-EXO, respectively. DAPI nuclear stain, blue; Phalloidin Texas Red-X, yellow; CD25 FITC, green; granzyme-B AF647, red. White arrow points to granule secretion from T cells as a result of activation. These images are representative of three independent experiments. **d**, Formation of CNP-CD8$^+$ T-cell aggregates viewed with an inverted-phase contrast microscope at 24 h, 48 h and 72 h. The black arrow points to a CNP–T cell aggregate (shown at higher magnification in the inset). Images are representative of three independent experiments.

Table 3 | Effect of CNP on T-cell proliferation and cell size as a function of time.

Group	Days	Fold expansion	Cell diameter (μm)
CNP	3	7.0 ± 0.1	9.3 ± 0.1
	5	22.4 ± 0.9	9.2 ± 0.1
	7	65.8 ± 5.2	8.1 ± 0.1
	14	191.9 ± 15.9	7.6 ± 0.0
TET-EXO	3	7.1 ± 0.2	8.6 ± 0.0
	5	17.7 ± 0.5	7.6 ± 0.0
	7	37.0 ± 1.3	6.5 ± 0.2
	14	44.1 ± 3.6	6.7 ± 0.0
DYNA-EXO	3	7.3 ± 0.2	8.8 ± 0.1
	5	20.8 ± 0.6	7.9 ± 0.0
	7	46.7 ± 1.9	6.8 ± 0.1
	14	77.1 ± 3.6	7.1 ± 0.1

indicated no significant differences in the percentage of activated T-cell populations (Supplementary Fig. 10a). Control groups significantly upregulated expression levels for CD25 and CD69 when compared to previous day 3 measurements using 1,000-fold less IL-2 (Supplementary Fig. 10b). In the context of T-cell function, intracellular granzyme-B levels increased for T cells previously cultured with DYNA-EXO$^+$ and TET-EXO$^+$ (by as much as 55% for the latter) compared to groups lacking the 1,000-fold excess IL-2 (Supplementary Fig. 10c), resulting in a significant enhancement in cell-specific cytolytic activity (Supplementary Fig. 10d). This is consistent with previous studies showing that IL-2 increases the cytolytic function in a dose-dependent manner during the primary activation of murine CD8$^+$ T cells *in vitro*[41].

In vivo anti-tumour activity of CNP-activated T cells

We evaluated the effects of CNPs for adoptive therapy against the B16 mouse melanoma model by transferring CD8$^+$ T cells via a single peritumoral injection. Mice were inoculated with the B16 tumour for ten days before T-cell injection. A significant delay in tumour growth at day 14 can be observed with animals adoptively transferred with CNP-cultured T cells compared with those without any treatment (Fig. 5a–c). Similar therapeutic effects with other platforms such as Dynabeads can be achieved, but only with 1,000-fold more IL-2.

To elucidate the immunological mechanisms behind the delayed tumour growth with CNP-cultured T cells, tumour-infiltrating lymphocytes (TILs) were harvested from the tumours of animals killed at day 14. A higher count of lymphocytes was detected in the tumour microenvironment[42], as indicated by the absolute number of isolated CD8$^+$ T cells per tumour in mice treated with CNP-stimulated cells versus control platforms (Fig. 5d). Tumour-infiltrating CD8$^+$ T-cell counts in the CNP group were similar to those for mice treated with cells previously expanded using DYNA-EXO$^+$, but at least ten times higher than in other control groups. T cells isolated from tumours treated with CNP or DYNA-EXO$^+$ were terminally differentiated into effectors, as indicated by a high proportion of lymphocytes expressing a CD44$^+$/CD62L$^-$ phenotype (Fig. 5e). Histological evaluation of tumour tissue in the CNP group confirmed evidence of lymphocyte infiltration and apoptosis in tumour cells (Fig. 5f, black arrow). This was also observed with tumour tissues isolated from DYNA-EXO$^+$ mice (Fig. 5f, dashed arrow), but to a lesser extent with tumours isolated from TET-EXO$^+$ mice. As expected, tissue samples from tumours in mice receiving no treatment showed the highest extent of cytologic

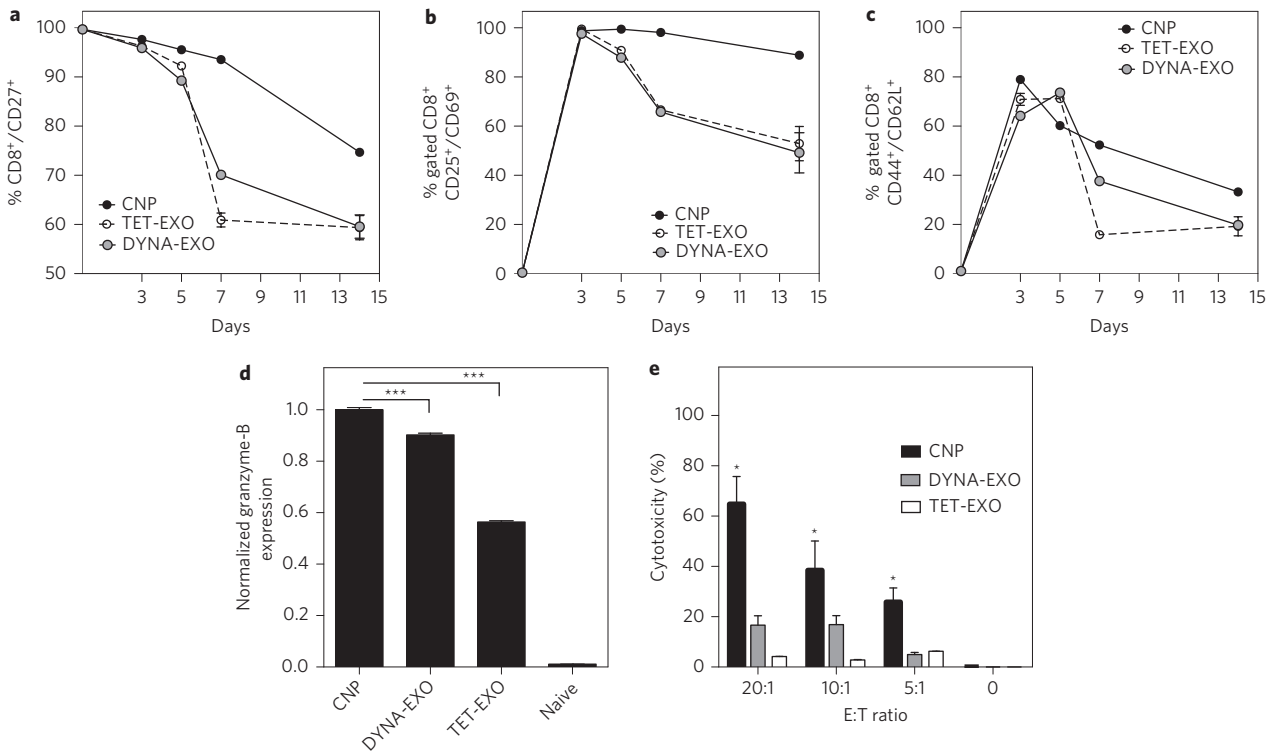

Figure 4 | Effect of CNPs on T-cell phenotype and cytolytic activity. Expression of survival and activation markers, as well as cytotoxic functions from CD8$^+$ T cells previously incubated with CNPs or control groups. **a–c**, Plots summarizing the percentage of CD8$^+$/CD27$^+$, CD25$^+$/CD69$^+$ and CD44$^+$/CD62L$^+$, respectively, in OT-1 CD8$^+$ T cells incubated with CNP versus controls as a function of time. **d**, Normalized expression of intracellular granzyme-B at day 3 in OT-1 CD8$^+$ T cells activated by CNP versus controls. ***$P < 0.0001$. **e**, Cytotoxic activity of OT-1 CD8$^+$ T cells towards B16 cells presenting MHC-I in the context of OVA. At an effector to target (E:T) ratio of 20:1, tumour cell lysis by T cells expanded with CNP is three times the cytolytic activity of T cells expanded using DYNA-EXO. *$P < 0.05$. All data are representative of three independent experiments. Error bars represent ± s.e.m. All gating of flow cytometry data was performed on live CD8$^+$ T cells.

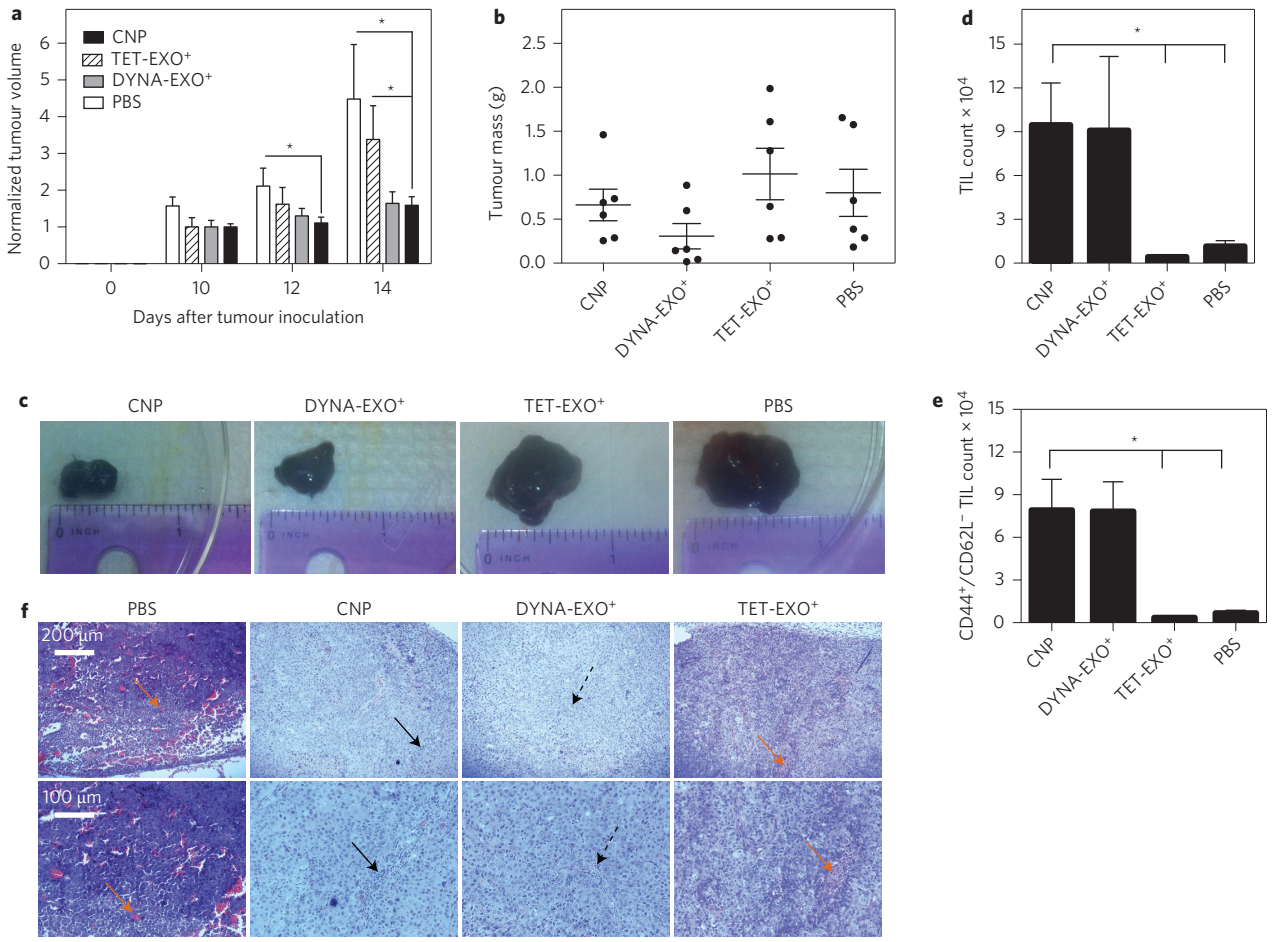

Figure 5 | Adoptive immunotherapy with CNP-expanded T cells delays the growth of tumours in a murine melanoma model. Tumour sizes were measured for two weeks in C57BL/6 mice inoculated with B16F10-OVA, and receiving OT-1 $CD8^+$ T cells previously activated with CNPs or controls containing 1,000-fold higher exogenous IL-2 concentrations. Mice were killed after two weeks, and the tumours were weighed then assessed for the presence of tumour-infiltrating lymphocytes. **a**, Delayed tumour growth in C57BL/6 mice previously inoculated with B16F10-OVA for ten days, and injected peritumorally with 1×10^6 OT-1 $CD8^+$ T cells per mouse. Tumour volumes were normalized to volumes measured at day 10 for each group. The results are mean values from six mice per group. **b**, Measurement of tumour mass for each group. Mice were killed directly before tumour mass determination. **c**, Representative tumour images from mice killed at day 14. **d**, Absolute number of activated T cells present in the tumour. Results are mean values from three tumours per group. **e**, Absolute number of $CD44^+/CD62L^-$ effector T cells present in the tumour. Results are mean values from three tumours per group. **f**, Haematoxylin and eosin stain of tumour samples from mice killed at the end of the study showing relative increase in lymphocyte infiltration in the CNP (black arrows) and DYNA-EXO^+ (dashed arrows) groups, and the presence of microvessels in samples isolated from the untreated (phosphate-buffered saline; PBS) and TET-EXO^+ groups (orange arrows). Error bars represent ±s.e.m. throughout. $^*P < 0.05$.

polymorphism (Fig. 5f, PBS group). One notable difference was also the decrease in microvessel density observed in samples isolated from the CNPs and DYNA-EXO^+; this was in addition to a decrease in tumour cell density (Fig. 5f). This decrease in tumour cell proliferation was consistent with the lack of new vasculature needed to supply the growing tumour mass.

Expansion of human $CD8^+$ T cells using CNPs

Expansion of antigen-specific T cells *in vitro* and adoptive transfer of these cells into patients could be an effective way to control chronic infections and malignancies such as melanoma. To demonstrate the efficacy of the CNP platform in expanding human T cells for adoptive cell therapy, we adapted the platform to expand human EBV-specific $CD8^+$ T cells. Figure 6 compares the expansion of EBV-specific $CD8^+$ T cells stimulated under three different conditions. CNPs were coated with either biotinylated EBV dimers (CNP/EBV) or biotinylated OKT-3 (equivalent to human anti-CD3) antibodies (CNP/OKT-3), while αCD28 antibodies were added to provide co-stimulation. To compare this system with stimulation by DCs under conventional conditions, DCs prepared from human peripheral blood mononuclear cells were pulsed with EBV peptide and maintained in IL-2 (100 U ml^{-1}) during T-cell stimulation. After a week of stimulation, cells were labelled with anti-CD8 and EBV tetramer to identify the EBV-specific population, together with a viability stain to monitor cell death. CNPs coated with EBV peptide loaded in human leukocyte antigen (HLA) were the most effective at expanding EBV-specific $CD8^+$ T cells, increasing EBV-specific frequencies fourfold compared to DC stimulation. In contrast, CNPs coated with high-affinity OKT-3 antibodies increased EBV-specific frequencies twofold compared to DCs, highlighting the utility of this system in increasing the avidity of weak-binding peptide/MHC-TCR interactions. Although the full adaptation of this system for clinical therapies is beyond the scope of this work, these results demonstrate the promise of the CNP platform in improving antigen-specific T-cell expansion for human adoptive cell therapies.

Conclusions

Because the T-cell response depends on the signals it receives from APCs, control over antigen presentation translates into control over

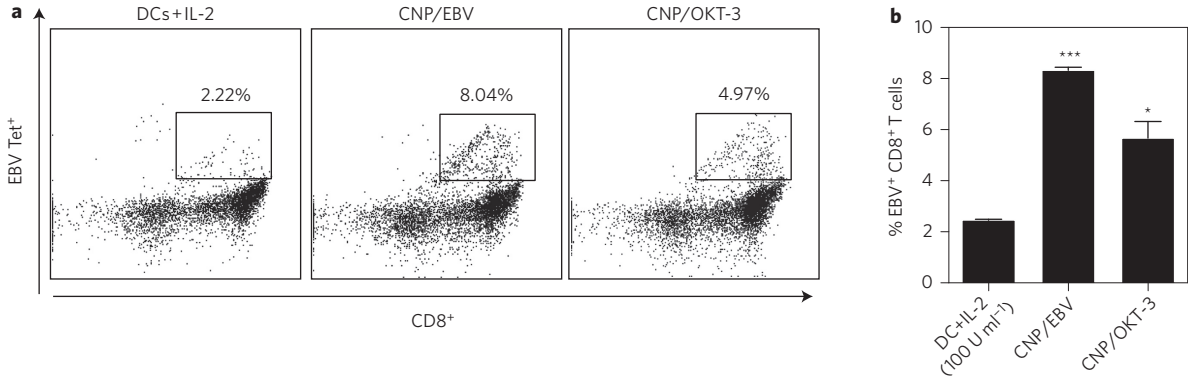

Figure 6 | Expansion of human T cells using CNPs. Measurement of human T-cell EBV$^+$/CD8$^+$ expansion using CNP, compared with a gold standard control (DCs), seven days after culture. **a**, Level of EBV$^+$ CD8$^+$ T-cell expansion measured by flow cytometry at day 7 in human CD8$^+$ T cells previously incubated with EBV pulsed DCs (100 U ml^{-1} soluble IL-2), CNP coated with OKT-3 and αCD28 antibodies (CNP/OKT-3), or CNP presenting EBV and αCD28 antibodies (CNP/EBV). The level of EBV$^+$/CD8$^+$ T-cell expansion was measured using EBV Tetramer (EBV Tet). **b**, Percentage of EBV$^+$/CD8$^+$ T cells measured on day 7 post-stimulation. Error bars represent ±s.e.m. $^*P < 0.05$, $^{***}P < 0.0001$.

T-cell stimulation and subsequent proliferation[43]. The composite system described here provides several parameters with which to engineer optimal antigen presentation using different T-cell antigens (peptide/MHC complexes and antibodies). In addition to the unique surface topology of CNTs mediating clustered antigen presentation, paracrine delivery of cytokines can be enabled in the system by coupling biodegradable polymeric nanoparticles encapsulated with the cytokine of interest. *In vivo*, paracrine signalling is pivotal to controlling lymphocyte response in the lymph node; in peripheral niches, directional cytokine secretion has been observed with antigen presentation[23,24]. Interestingly, the CNP antigen-presentation system offers the potential for enhancing the proliferation and function of T cells to a level that would require at least 1,000-fold less soluble IL-2 under conventional culture conditions. Finally, magnetic separation via magnetite co-encapsulated in the particles enables easy isolation and enrichment of activated T cells for adoptive transfer.

Ease of use, modularity and material availability are attractive features for a general, modular, off-the-shelf therapeutic device. This is in addition to the potential for large-scale manufacturing, which can translate into significant cost reductions. Irrespective of their scale or nature, all cell culture systems supply exogenous bioactive factors by direct addition to the culture medium. Cost is particularly an issue during prolonged culture and when there is a requirement for complex cocktails to expand and differentiate cells to a specific endpoint[44,45]. Carbon nanotubes and biodegradable polymers are currently available on a large scale, predominantly for use in the energy or pharmaceutical excipient sectors. Unlike live cells, these engineered systems can be stored for extended periods of time. Proteins attached to the surfaces of CNTs are stabilized against denaturation[33]. The cytokine dose is lower because of the high local concentrations and the encapsulated format, which is also more stable in the case of free IL-2, because it is protected from physiological media and released in a paracrine fashion near its target[30]. Another factor that influences cost efficiency is the specificity. Exogenously supplied factors can support the viability or growth of undesired cell populations, which can then compete with the culture of target cell types or influence their function. A relatively unexplored strategy to improve the specificity of a cell culture is to target stimulatory factors to cell types of interest using biodegradable micro- or nanoparticles. This approach would enable spatial and temporal control of local T-cell stimulation. In summary, the composite aAPC system discussed here may offer greater stability and thus a more economical way to generate T cells for use than relying on live cells.

Materials and methods

Preparation of PLGA nanoparticles. A 50 µl volume of recombinant proleukin human IL-2 (Novartis) at 1.2 mg ml^{-1} in PBS was added dropwise to a vortexing solution of PLGA 50:50 (100 mg) with an inherent viscosity of 0.59 dl g^{-1} (Lactel Polymers) and hydrophobic magnetite (18 mg) dissolved in 2 ml chloroform (Thermo Scientific). The mixture was added dropwise to 3.2 ml of a vortexing solution of 5% polyvinyl alcohol (PVA, Sigma-Aldrich) with $M_{W,ave}$ = 30–70 kDa and 1,2-distearoyl-sn-glycero-3-phosphoethanolamine (DSPE)-PEG-biotin (4.14 mg/0.828 ml) (Avanti Polar Lipid). The mixture was then sonicated three times for 10 s at 38% amplitude (TEKMAR VCW 400 W). The solution was added dropwise to 100 ml of 0.2% PVA, and left stirring for 3 h to evaporate the solvent. Particles were collected by centrifugation at 12,000 r.p.m. for 15 min at 4 °C, then washed three times with deionized water. The particles were lyophilized and stored at –20 °C.

T-cell stimulation studies. OT-1 mice were bred, maintained and screened in the Malone Engineering Center at Yale University. Splenocytes were isolated from the spleen of OT-1 mice (aged 6–8 weeks) after depletion of erythrocytes by hypotonic lysis. CD8$^+$ T cells were isolated using a CD8$^+$ negative selection kit (StemCell). CD8$^+$ T cells were resuspended in cell media composed of RPMI 1640 supplemented with FBS (10%), L-glutamine (1%), HEPES buffer (1%), non-essential amino acids, 2-ME (0.1%) and penicillin (2%), and stored at 4 °C before use. Equimolar amounts (2.1 nM total) of biotinylated MHC-I (H-2K^b loaded with SIINFEKL peptides) and αCD28 (BD Biosciences) were added to the ^{N}CNT suspension, and allowed to mix for 1 h at room temperature. As a final step, PLGA nanoparticles (625 µg ml^{-1}) were added to the mixture and allowed to bind for 30 min. The mixture was then diluted in cell media (1:5) and added to an equal volume of CD8$^+$ T cells (5×10^5 cells ml^{-1}) in a 24-well plate. For control groups, streptavidin-coated Dynabeads (Invitrogen) were added at a final concentration of 1×10^6 particles ml^{-1} using cell culture conditions similar to those for CNPs. The cells were then incubated at 37 °C. After three days of culture, samples were purified using magnetic separation to isolate activated T cells, counted, and sized using a Multisizer 3 (Beckman Coulter) at 1:400 dilution, then processed for analysis. For long-term expansion studies, T cells collected at day 3 were re-stimulated using the same quantity of soluble MHC-I and αCD28, together with exogenous IL-2 or PLGA nanoparticles depending on the groups. We chose to activate the cells using CNPs for the first three days to avoid effects related to T-cell exhaustion (Supplementary Fig. 11). At days 5, 7 and 14, T cells were purified using magnetic separation, counted and sized, then re-stimulated using conditions similar to those for day 3.

***In vivo* melanoma study.** C57BL/6 mice were accommodated in autoclaved micro-isolator cages housed in a positive-pressure containment rack, and maintained under the guidelines of an approved protocol from the Yale University Institutional Animal Care and Use Committee. Mice were randomly assigned to groups of six animals each. The xenografts of melanoma were developed by subcutaneously implanting 5×10^6 B16F10-OVA cells in the right flank of the mice. After 10 days of tumour inoculation, each mouse was treated with activated OT-1 CD8$^+$ T cells by direct injection into the tumour. The tumour inhibition activity was determined with the tumour volume, which was calculated using the equation $V = w^2 \times l/2$, where w and l are the width and length of the tumour as measured by a caliper. All animals were killed at the same time point for consistent comparison of tumour sizes for all groups, or when a mouse met any of the following conditions: (1) 15% loss in initial bodyweight; (2) tumour size ≥ 1.5 cm in any dimension; (3) mouse becoming lethargic, sick or unable to feed; (4) mouse developing an ulcerated tumour.

Human T-cell expansion study. $CD8^+$ T cells were isolated from human peripheral blood mononuclear cells (PBMCs) or leukopak of healthy HLA-$A2^+$ individuals via negative immunoselection (Miltenyi Biotech) according to the manufacturer's instructions. Equimolar amounts of either biotinylated HLA-A2 dimer (BD Biosciences) loaded with EBV peptide or biotinylated human anti-CD3 (OKT3, eBiosciences) and αCD28 (Biolegend) were added to the ^{N}CNT suspension, and allowed to mix for 1 h at room temperature. IL-2 encapsulating PLGA nanoparticles (31.25 μg ml^{-1} final) were added to the mixture and allowed to bind for 30 min at room temperature. CNP (1.25 μg ml^{-1}) was added to 1×10^6 $CD8^+$ T cells per plate in a 96-well plate.

Received 9 December 2012; accepted 30 June 2014; published online 3 August 2014

References

1. Waldmann, T. A. Immunotherapy: past, present and future. *Nature Med.* **9,** 269–277 (2003).
2. Dudley, M. E. & Rosenberg, S. A. Adoptive-cell-transfer therapy for the treatment of patients with cancer. *Nature Rev. Cancer* **3,** 666–675 (2003).
3. Zemon, H. An artificial solution for adoptive immunotherapy. *Trends Biotechnol.* **21,** 418–420 (2003).
4. Brentjens, R. J. *et al.* CD19-targeted T cells rapidly induce molecular remissions in adults with chemotherapy-refractory acute lymphoblastic leukemia. *Science Transl. Med.* **5,** 177ra38 (2013).
5. Robbins, P. F. *et al.* Tumor regression in patients with metastatic synovial cell sarcoma and melanoma using genetically engineered lymphocytes reactive with NY-ESO-1. *J. Clin. Oncol.* **29,** 917–924 (2011).
6. Grupp, S. A. *et al.* Chimeric antigen receptor-modified T cells for acute lymphoid leukemia. *N. Engl. J. Med.* **368,** 1509–1518 (2013).
7. Murphy, K., Travers, P. & Walport, M. *Janeway's Immunobiology* (Garland Science, 2008).
8. Kim, J. V., Latouche, J.-B., Rivière, I. & Sadelain, M. The ABCs of artificial antigen presentation. *Nature Biotechnol.* **22,** 403–410 (2004).
9. Steenblock, E. R., Wrzesinski, S. H., Flavell, R. A. & Fahmy, T. M. Antigen presentation on artificial acellular substrates: modular systems for flexible, adaptable immunotherapy. *Expert Opin. Biol. Ther.* **9,** 451–464 (2009).
10. Kropshofer, H. *et al.* Tetraspan microdomains distinct from lipid rafts enrich select peptide-MHC class II complexes. *Nature Immunol.* **3,** 61–68 (2002).
11. Fooksman, D. R., Grönvall, G. K., Tang, Q. & Edidin, M. Clustering class I MHC modulates sensitivity of T cell recognition. *J. Immunol.* **176,** 6673–6680 (2006).
12. Andersen, P. S., Menné, C., Mariuzza, R. A., Geisler, C. & Karjalainen, K. A response calculus for immobilized T cell receptor ligands. *J. Biol. Chem.* **276,** 49125–49132 (2001).
13. González, P. A. *et al.* T cell receptor binding kinetics required for T cell activation depend on the density of cognate ligand on the antigen-presenting cell. *Proc. Natl Acad. Sci. USA* **102,** 4824–4829 (2005).
14. Grakoui, A. *et al.* The immunological synapse: a molecular machine controlling T cell activation. *Science* **285,** 221–227 (1999).
15. Monks, C. R., Freiberg, B. A., Kupfer, H., Sciaky, N. & Kupfer, A. Three-dimensional segregation of supramolecular activation clusters in T cells. *Nature* **395,** 82–86 (1998).
16. Cemerski, S. *et al.* The stimulatory potency of T cell antigens is influenced by the formation of the immunological synapse. *Immunity* **26,** 345–355 (2007).
17. Li, Q.-J. *et al.* CD4 enhances T cell sensitivity to antigen by coordinating Lck accumulation at the immunological synapse. *Nature Immunol.* **5,** 791–799 (2004).
18. Oelke, M. *et al. Ex vivo* induction and expansion of antigen-specific cytotoxic T cells by HLA-Ig-coated artificial antigen-presenting cells. *Nature Med.* **9,** 619–624 (2003).
19. Prakken, B. *et al.* Artificial antigen-presenting cells as a tool to exploit the immune 'synapse'. *Nature Med.* **6,** 1406–1410 (2000).
20. Zitvogel, L. *et al.* Eradication of established murine tumors using a novel cell-free vaccine: dendritic cell derived exosomes. *Nature Med.* **4,** 594–600 (1998).
21. Steenblock, E. R. & Fahmy, T. M. A comprehensive platform for *ex vivo* T-cell expansion based on biodegradable polymeric artificial antigen-presenting cells. *Mol. Ther.* **16,** 765–772 (2008).
22. Oosten, L. E. M. *et al.* Artificial antigen-presenting constructs efficiently stimulate minor histocompatibility antigen-specific cytotoxic T lymphocytes. *Blood* **104,** 224–226 (2004).
23. Sabatos, C. A. *et al.* A synaptic basis for paracrine interleukin-2 signaling during homotypic T cell interaction. *Immunity* **29,** 238–248 (2008).
24. Huse, M., Quann, E. J. & Davis, M. M. Shouts, whispers and the kiss of death: directional secretion in T cells. *Nature Immunol.* **9,** 1105–1111 (2008).
25. Ye, Q. *et al.* Engineered artificial antigen presenting cells facilitate direct and efficient expansion of tumor infiltrating lymphocytes. *J. Transl. Med.* **9,** 131 (2011).
26. Malek, T. R. The biology of interleukin-2. *Annu. Rev. Immunol.* **26,** 453–479 (2008).
27. Fadel, T. R. & Fahmy, T. M. Immunotherapy applications of carbon nanotubes: from design to safe applications. *Trends Biotechnol.* **32,** 198–209 (2014).
28. Zanello, L. P., Zhao, B., Hu, H. & Haddon, R. C. Bone cell proliferation on carbon nanotubes. *Nano Lett.* **6,** 562–567 (2006).
29. Nayak, T. R. *et al.* Thin films of functionalized multiwalled carbon nanotubes as suitable scaffold materials for stem cells proliferation and bone formation. *ACS Nano* **4,** 7717–7725 (2010).
30. Steenblock, E. R., Fadel, T., Labowsky, M., Pober, J. S. & Fahmy, T. M. An artificial antigen-presenting cell with paracrine delivery of IL-2 impacts the magnitude and direction of the T cell response. *J. Biol. Chem.* **286,** 34883–34892 (2011).
31. Chen, Y. *et al.* Low-defect, purified, narrowly (*n,m*)-dispersed single-walled carbon nanotubes grown from cobalt-incorporated MCM-41. *ACS Nano* **1,** 327–336 (2007).
32. Fadel, T. R. *et al.* Enhanced cellular activation with single walled carbon nanotube bundles presenting antibody stimuli. *Nano Lett.* **8,** 2070–2076 (2008).
33. Fadel, T. R. *et al.* Adsorption of multimeric T cell antigens on carbon nanotubes: effect on protein structure and antigen-specific T cell stimulation. *Small* **9,** 666–672 (2013).
34. Hogquist, K. A. *et al.* T cell receptor antagonist peptides induce positive selection. *Cell* **76,** 17–27 (1994).
35. Fadel, T. R. *et al.* Clustering of stimuli on single-walled carbon nanotube bundles enhances cellular activation. *Langmuir* **26,** 5645–5654 (2010).
36. Park, J. *et al.* Enhancement of surface ligand display on PLGA nanoparticles with amphiphilic ligand conjugates. *J. Control. Rel.* **156,** 109–115 (2011).
37. Fahmy, T. M., Samstein, R. M., Harness, C. C. & Mark Saltzman, W. Surface modification of biodegradable polyesters with fatty acid conjugates for improved drug targeting. *Biomaterials* **26,** 5727–5736 (2005).
38. Ragheb, R. R. T. *et al.* Induced clustered nanoconfinement of superparamagnetic iron oxide in biodegradable nanoparticles enhances transverse relaxivity for targeted theranostics. *Magn. Reson. Med.* **70,** 1748–1760 (2013).
39. Cheng, L. E., Ohlén, C., Nelson, B. H. & Greenberg, P. D. Enhanced signaling through the IL-2 receptor in CD8+ T cells regulated by antigen recognition results in preferential proliferation and expansion of responding CD8+ T cells rather than promotion of cell death. *Proc. Natl Acad. Sci. USA* **99,** 3001–3006 (2002).
40. Labowsky, M. & Fahmy, T. M. Diffusive transfer between two intensely interacting cells with limited surface kinetics. *Chem. Eng. Sci.* **74,** 114–123 (2012).
41. Janas, M. L., Groves, P., Kienzle, N. & Kelso, A. IL-2 regulates perforin and granzyme gene expression in CD8+ T cells independently of its effects on survival and proliferation. *J. Immunol.* **175,** 8003–8010 (2005).
42. Rabinovich, G. A., Gabrilovich, D. & Sotomayor, E. M. Immunosuppressive strategies that are mediated by tumor cells. *Annu. Rev. Immunol.* **25,** 267–296 (2007).
43. Pardoll, D. M. Spinning molecular immunology into successful immunotherapy. *Nature Rev. Immunol.* **2,** 227–238 (2002).
44. Suter, D. M. & Krause, K-H. Neural commitment of embryonic stem cells: molecules, pathways and potential for cell therapy. *J. Pathol.* **215,** 355–368 (2008).
45. McIntosh, K. *et al.* The immunogenicity of human adipose-derived cells: temporal changes *in vitro*. *Stem Cells* **24,** 1246–1253 (2006).

Acknowledgements

This work was supported in part by a National Science Foundation Career Award (0747577) to T.M.F. and in part by a National Institutes of Health Autoimmunity Center of Excellence Pilot Award (U19 AI056363, to T.M.F. and K.H.) and a Yale Specialized Programs of Research Excellence (SPORE) Investigator Pilot Award (to T.M.F.) and in part by the Yale SPORE in Skin Cancer (grant no. 1 P50 CA121974). The authors thank J. Alderman and R. Flavell for helpful critique, and M. Sznol, R. Tigelaar and M. Bosenberg (Yale Cancer Center), as well as P. De Sousa (University of Edinburgh), for technical comments regarding adoptive therapy. The authors also thank P. Van Tassel for technical advice regarding CNT preparation.

Author contributions

T.R.F. and T.M.F. designed all of the experiments for this study. R.R synthesized the magnetite and fabricated the polymer nanoparticles. N.L. synthesized the carbon nanotubes. S.J. synthesized the biotinylated MHC-I. T.R.F., L.D.P. and G.L.H. characterized the carbon nanotubes. T.R.F. and R.R. characterized the particles and the CNP system. R.R. characterized the magnetic properties of the PLGA nanoparticles and CNPs. T.R.F. performed inverted, fluorescence and FRET imaging. T.R.F. performed *in vitro* characterization experiments and FACS analyses. T.R.F., F.S. and E.H. performed the studies on T-cell cytotoxicity. T.R.F., F.S. and D.K. characterized the tumour-infiltrating lymphocytes. F.S., N.V., and J.G. performed the human T cell expansion experiments. T.R.F. and D.K. performed the *in vivo* experiments. T.M.F. conceived the formulations. T.R.F. wrote the manuscript. T.M.F., R.R., D.K., F.S., E.H., L.D.P., and K.C.H. edited the manuscript.

Additional information

Supplementary information is available in the online version of the paper. Reprints and permissions information is available online at www.nature.com/reprints. Correspondence and requests for materials should be addressed to T.M.F.

Competing financial interests

The authors declare no competing financial interests.